INTERNATIONAL JOURNAL FOR NUMERICAL METHODS IN FLUIDS, VOL. 23, 485–501 (1996)

NUMERICAL INVESTIGATION OF TURBULENT SHALLOW RECIRCULATING FLOWS BY A QUASI-THREE-DIMENSIONAL $k-\epsilon$ MODEL

C. W. LI AND T. S. YU

Department of Civil and Structural Engineering, Hong Kong Polytechnic University, Hong Kong

A quasi-three-dimensional multilayer $k-\epsilon$ model has been developed to simulate turbulent recirculating flows behind a sudden expansion in shallow waters. The model accounts for the vertical variation in the flow quantities and eliminates the problem of closure for the effective stresses resulting from the depth integration of the non-linear convective accelerations found in the widely used depth-integrated models. The governing equations are split into three parts in the finite difference solution: advection, dispersion and propagation. The advection part is solved using the four-node minimax–characteristics method. The dispersion and propagation parts are treated by the central difference method, the former being solved explicitly and the latter implicitly using the Gauss–Seidel iteration method. The relative effect of bed-generated turbulence and transverse shear-generated turbulence on the recirculating flow has been studied in detail. In comparison with the results computed by the depth-integrated $k-\epsilon$ model, the results computed by the present model are found to be closer to the reported data.

KEY WORDS: shallow recirculating flow; multilayer model; turbulence model

INTRODUCTION

Turbulent free surface, shallow water flow problems are often encountered in hydraulic engineering. The flows are usually characterized by a three-dimensional varition in flow magnitude but a two-dimensional variation in flow directions (mainly in the horizontal directions), with the vertical currents small and negligible. In the presence of recirculation, such as the flow behind a sudden expansion in an open channel, the turbulence and hence the mean flow are strongly affected by the influence of bed friction and transverse shear. In modelling recirculating flow the closure approximation of the effective stresses is important and a sophisticated turbulence model such as the $k-\epsilon$ model[1] is required.

Since free surface flow directions are usually two-dimensional, depth- integrated models are widely used in simulating this phenomenon. Rastogi and Rodi[2] developed the first depth-integrated $k-\epsilon$ model and studied the recirculating flow generated by a side discharge into an open channel. Booij[3] and Yu and Zhang[4] presented several different versions of the $k-\epsilon$ model. In these models the rigid lid assumption was employed. This assumption allows only a linear variation in the water surface and wave formation at the water surface will be suppressed. In contrast, Chapman and Kuo[5] developed a depth-integrated $k-\epsilon$ model which allows free surface variation. When simulating recirculating flows, these depth-integrated $k-\epsilon$ models were found to underpredict the reattachment length. It is widely accepted that this is due to the inadequacy of the $k-\epsilon$ model for turbulence.

However, in flow simulation using depth-integrated models, the effect of the vertical variation in the flow quantities has not been explicitly accounted for. In particular, the problem of closure of the

CCC 0271–2091/96/0505485–17

Received November 1995
Revised January 1996

effective stresses resulting from the depth integration of the non-linear convective accelerations has not been addressed. This may be part of the cause of the inaccuracy of the models.

To improve the prediction of shallow recirculating flow, a quasi-three-dimensional multilayer $k-\epsilon$ model (M$k\epsilon$ model) is developed in the present work. For the numerical scheme the split operator method is used.[6] The governing equations are split into three parts in the solution: advection, dispersion and propagation. The advection part is solved using the four-node minimax–characteristics method.[7] The dispersion and propagation parts are treated by the central difference method;[8] the former will be solved explicitly and the latter implicitly using the Gauss–Seidel iteration method. The relative effect of bed-generated turbulence and transverse shear-generated turbulence on the recirculating flow will be studied in detail. The results computed by the present model will be compared with those computed by the depth-integrated $k-\epsilon$ model (D$k\epsilon$ model) as well as with the experimental data of Babarutsi *et al.*[9]

GOVERNING EQUATIONS

By assuming hydrostatic pressure and neglecting the vertical velocity and the effects of wind and Coriolis force, the three-dimensional multilayer equations of motions can be obtained by integrating the governing equations vertically across each layer (see e.g. Reference 10). The vertically integrated effective stress tensors are represented by the Boussinesq eddy viscosity expressions.[5] For layer k the equations are as follows: x-momentum equation

$$\frac{\partial q_{kx}}{\partial t}+U_k\frac{\partial q_{kx}}{\partial x}+V_k\frac{\partial q_{kx}}{\partial y}=\frac{\partial}{\partial x}\left(2h_k\nu_k\frac{\partial U_k}{\partial x}\right)+\frac{\partial}{\partial y}\left(h_k\nu_k\frac{\partial U_k}{\partial y}\right)+\frac{\partial}{\partial y}\left(h_k\nu_k\frac{\partial V_k}{\partial x}\right)$$
$$+h_k\frac{\partial}{\partial z}\left(\nu_k\frac{\partial U_k}{\partial z}\right)-gh_k\frac{\partial \eta}{\partial x}$$
$$+\left(\frac{\partial}{\partial x}\int_{h_k}(U_k-\bar{U}_k)^2\,\mathrm{d}z+\frac{\partial}{\partial y}\int_{h_k}(U_k-\bar{U}_k)(V_k-\bar{V}_k)\,\mathrm{d}z\right), \tag{1}$$

y-momentum equation

$$\frac{\partial q_{ky}}{\partial t}+U_k\frac{\partial q_{ky}}{\partial x}+V_k\frac{\partial q_{ky}}{\partial y}=\frac{\partial}{\partial x}\left(h_k\nu_k\frac{\partial U_k}{\partial y}\right)+\frac{\partial}{\partial x}\left(h_k\nu_k\frac{\partial V_k}{\partial x}\right)+\frac{\partial}{\partial y}\left(2h_k\nu_k\frac{\partial V_k}{\partial y}\right)$$
$$+h_k\frac{\partial}{\partial z}\left(\nu_k\frac{\partial V_k}{\partial z}\right)-gh_k\frac{\partial \eta}{\partial y}$$
$$+\left(\frac{\partial}{\partial x}\int_{h_k}(U_k-\bar{U}_k)(V-\bar{V}_k)\,\mathrm{d}z+\frac{\partial}{\partial y}\int_{h_k}(V_k-\bar{V}_k)^2\,\mathrm{d}z\right) \tag{2}$$

and continuity equation

$$\frac{\partial \eta}{\partial t}+\sum_1^N\left(\frac{\partial q_{kx}}{\partial x}+\frac{\partial q_{ky}}{\partial y}\right)=0, \tag{3}$$

where x is the longitudinal co-ordinate direction, y is the transverse co-ordinate direction, z is the vertical co-ordinate direction, U_k is the longitudinal velocity in layer k, V_k is the transverse velocity in layer k, h_k is the thickness of layer k, N is the total number of layers, η is the free surface elevation, H is the still water depth, $H+\eta$ is the sum of the thicknesses of each layer ($H+\eta=\sum_1^N h_k$), ν_k is the dynamic viscosity in layer k, q_{kx} is the longitudinal flow rate in layer k ($q_{kx}=U_kh_k$), q_{ky} is the transverse flow rate in layer ($q_{ky}=V_kh_k$), t is the time and g is the acceleration due to gravity. The

longitudinal and transverse surface stresses τ_{sx} and τ_{sy}, the longitudinal and transverse bottom stresses τ_{bx} and τ_{by} and shear stresses next to the wall boundaries, τ_w, will be specified in the section on 'Boundary conditions'.

The last terms in equations (1) and (2) are called momentum dispersion terms. These terms are due to the vertical non-uniformities of the mean flow quantities in every layer k. When the integrated model ($N=1$) is used, the vertical non-uniformities of the mean flow quantities may be large and cannot be neglected. However, when the water flow is cut into a sufficient number of layers, U_k and V_k are almost uniform in every layer k and thus the momentum dispersion terms become very small and are neglected in this study.

EFFECTIVE STRESS CLOSURE ($k-\epsilon$ EQUATIONS)

The eddy viscosity ν_k appearing in equations (1) and (2) is given by

$$\nu_k = C_\mu \frac{k_k^2}{\epsilon_k}, \tag{4}$$

where k_k is the turbulence kinetic energy of layer k and ϵ_k is the turbulence dissipation rate of layer k. The k-equation is

$$\frac{\partial k_k}{\partial t} + U_k \frac{\partial k_k}{\partial x} + V_k \frac{\partial k_k}{\partial y} = \frac{\partial}{\partial x}\left(\frac{\nu_k}{\sigma_k}\frac{\partial k_k}{\partial x}\right) + \frac{\partial}{\partial y}\left(\frac{\nu_k}{\sigma_k}\frac{\partial k_k}{\partial y}\right) + \frac{\partial}{\partial z}\left(\frac{\nu_k}{\sigma_k}\frac{\partial k_k}{\partial z}\right) - \epsilon_k + \nu_k\left[2\left(\frac{\partial U_k}{\partial x}\right)^2 + 2\left(\frac{\partial V_k}{\partial y}\right)^2 + \left(\frac{\partial U_k}{\partial z}\right)^2 + \left(\frac{\partial V_k}{\partial z}\right)^2 + \left(\frac{\partial U_k}{\partial y} + \frac{\partial V_k}{\partial x}\right)^2\right]. \tag{5}$$

The ϵ-equation is

$$\frac{\partial \epsilon_k}{\partial t} + U_k \frac{\partial \epsilon_k}{\partial x} + V_k \frac{\partial \epsilon_k}{\partial y} = \frac{\partial}{\partial x}\left(\frac{\nu_k}{\sigma_\epsilon}\frac{\partial \epsilon_k}{\partial x}\right) + \frac{\partial}{\partial y}\left(\frac{\nu_k}{\sigma_\epsilon}\frac{\partial \epsilon_k}{\partial y}\right) + \frac{\partial}{\partial z}\left(\frac{\nu_k}{\sigma_\epsilon}\frac{\partial \epsilon_k}{\partial z}\right) - C_{2\epsilon}\frac{\epsilon_k^2}{k_k} + C_{1\epsilon}\frac{\epsilon_k}{k_k}\nu_k\left[2\left(\frac{\partial U_k}{\partial x}\right)^2 + 2\left(\frac{\partial V_k}{\partial y}\right)^2 + \left(\frac{\partial U_k}{\partial z}\right)^2 + \left(\frac{\partial V_k}{\partial z}\right)^2 + \left(\frac{\partial U_k}{\partial y} + \frac{\partial V_k}{\partial x}\right)^2\right], \tag{6}$$

where $C_\mu = 0{\cdot}09$, $C_{1\epsilon} = 1{\cdot}44$, $C_{2\epsilon} = 1{\cdot}92$, $\sigma_k = 1{\cdot}0$ and $\sigma_\epsilon = 1{\cdot}3$ as recommended by Launder and Spalding.[11] The four terms

$$\nu_k\left(\frac{\partial U_k}{\partial z}\right)^2, \quad \nu_k\left(\frac{\partial V_k}{\partial z}\right)^2, \quad C_{1\epsilon}\frac{\epsilon_k}{k_k}\nu_k\left(\frac{\partial U_k}{\partial z}\right)^2 \quad \text{and} \quad C_{1\epsilon}\frac{\epsilon_k}{k_k}\nu_k\left(\frac{\partial V_k}{\partial z}\right)^2$$

generate k and ϵ at each layer owing to the vertical gradients of U and V, while the two terms

$$\frac{\partial}{\partial z}\left(\frac{\nu_k}{\sigma_k}\frac{\partial k_k}{\partial z}\right) \quad \text{and} \quad \frac{\partial}{\partial z}\left(\frac{\nu_k}{\sigma_\epsilon}\frac{\partial \epsilon_k}{\partial z}\right)$$

diffuse k and ϵ vertically. In addition, the values of k and ϵ generated at the bottom layer and the surface layer, as well as the values of k and ϵ next to the wall boundaries, will be specified in the section on 'Boundary conditions'. Therefore k and ϵ generated at every layer will be diffused vertically and the above equations do not need to contain the empirical source terms P_{kv} and $P_{\epsilon V}$ appearing in the depth-integrated $k-\epsilon$ equations (see Appendix).

NUMERICAL SCHEME

In this study the split operator approach[6,12] is used in the solution. At each time step the equations are split into three steps—advection, diffusion, propagation and source terms—as follows.

Advection step

$$\frac{q_{kx}^{n+1/3} - q_{kx}^{n}}{\Delta t} + U_k \frac{\partial q_{kx}}{\partial x} + V_k \frac{\partial q_{kx}}{\partial y} = 0, \tag{7}$$

$$\frac{q_{ky}^{n+1/3} - q_{ky}^{n}}{\Delta t} + U_k \frac{\partial q_{ky}}{\partial x} + V_k \frac{\partial q_{ky}}{\partial y} = 0, \tag{8}$$

$$\frac{k_k^{n+1/3} - k_k^{n}}{\Delta t} + U_k \frac{\partial k_k}{\partial x} + V_k \frac{\partial k_k}{\partial y} = 0, \tag{9}$$

$$\frac{\epsilon_k^{n+1/3} - \epsilon_k^{n}}{\Delta t} + U_k \frac{\partial \epsilon_k}{\partial x} + V_k \frac{\partial \epsilon_k}{\partial y} = 0. \tag{10}$$

In the advection step a four-node minimax–characteristics scheme proposed by Li[7] is employed to solve the equations of pure advection. Details of the solution method for advection are given in the next section.

Diffusion step

$$\frac{q_{kx}^{n+2/3} - q_{kx}^{n+1/3}}{\Delta t} = \frac{\partial}{\partial x}\left(2h_k \nu_k \frac{\partial U_k}{\partial x}\right) + \frac{\partial}{\partial y}\left(h_k \nu_k \frac{\partial U_k}{\partial y}\right) + \frac{\partial}{\partial y}\left(h_k \nu_k \frac{\partial V_k}{\partial x}\right) + h_k \frac{\partial}{\partial z}\left(\nu_k \frac{\partial U_k}{\partial z}\right), \tag{11}$$

$$\frac{q_{ky}^{n+2/3} - q_{ky}^{n+1/3}}{\Delta t} = \frac{\partial}{\partial x}\left(h_k \nu_k \frac{\partial U_k}{\partial y}\right) + \frac{\partial}{\partial x}\left(h_k \nu_k \frac{\partial V_k}{\partial x}\right) + \frac{\partial}{\partial y}\left(2h_k \nu_k \frac{\partial V_k}{\partial y}\right) + h_k \frac{\partial}{\partial z}\left(\nu_k \frac{\partial V_k}{\partial z}\right), \tag{12}$$

$$\frac{k_k^{n+2/3} - k_k^{n+1/3}}{\Delta t} = \frac{\partial}{\partial x}\left(\frac{\nu_k}{\sigma_k}\frac{\partial k_k}{\partial x}\right) + \frac{\partial}{\partial y}\left(\frac{\nu_k}{\sigma_k}\frac{\partial k_k}{\partial y}\right) + \frac{\partial}{\partial z}\left(\frac{\nu_k}{\sigma_k}\frac{\partial k_k}{\partial z}\right), \tag{13}$$

$$\frac{\epsilon_k^{n+2/3} - \epsilon_k^{n+1/3}}{\Delta t} = \frac{\partial}{\partial x}\left(\frac{\nu_k}{\sigma_\epsilon}\frac{\partial \epsilon_k}{\partial x}\right) + \frac{\partial}{\partial y}\left(\frac{\nu_k}{\sigma_\epsilon}\frac{\partial \epsilon_k}{\partial y}\right) + \frac{\partial}{\partial z}\left(\frac{\nu_k}{\sigma_\epsilon}\frac{\partial \epsilon_k}{\partial z}\right). \tag{14}$$

In the diffusion step the simple forward time, centred space scheme[8] is used, because the diffusion terms are generally small in horizontal flows.

Propagation and source terms step

$$\frac{q_{kx}^{n+1} - q_{kx}^{n+2/3}}{\Delta t} = -gh_k \frac{\partial \eta}{\partial x}, \tag{15}$$

$$\frac{q_{ky}^{n+1} - q_{ky}^{n+2/3}}{\Delta t} = -gh_k \frac{\partial \eta}{\partial y}, \tag{16}$$

$$\frac{\eta^{n+1} - \eta^n}{\Delta t} = -\sum_1^N \left(\frac{\partial q_{kx}}{\partial x} + \frac{\partial q_{ky}}{\partial y} \right), \tag{17}$$

$$\frac{k_k^{n+1} - k_k^{n+2/3}}{\Delta t} = \nu_k \left[2\left(\frac{\partial U_k}{\partial x}\right)^2 + 2\left(\frac{\partial V_k}{\partial y}\right)^2 + \left(\frac{\partial U_k}{\partial z}\right)^2 + \left(\frac{\partial V_k}{\partial z}\right)^2 + \left(\frac{\partial U_k}{\partial y} + \frac{\partial V_k}{\partial x}\right)^2 \right] - \epsilon_k, \tag{18}$$

$$\frac{\epsilon_k^{n+1} - \epsilon_k^{n+2/3}}{\Delta t} = C_{1\epsilon} \frac{\epsilon_k}{k_k} \nu_k \left[2\left(\frac{\partial U_k}{\partial x}\right)^2 + 2\left(\frac{\partial V_k}{\partial y}\right)^2 + \left(\frac{\partial U_k}{\partial z}\right)^2 + \left(\frac{\partial V_k}{\partial z}\right)^2 + \left(\frac{\partial U_k}{\partial y} + \frac{\partial V_k}{\partial x}\right)^2 \right] - C_{2\epsilon} \frac{\epsilon_k^2}{k_k}. \tag{19}$$

Equations (18) and (19) are solved explicitly and an implicit scheme is applied to solved equations (15)–(17). The three equations are decoupled through two procedures. First, the unknowns of flow rate at time level $n+1$ are eliminated by differentiating equations (15) and (16) with respect to x and y. Second, the resulting Poisson-type equation with essential boundary conditions is solved using the Gauss–Seidel iteration method. The finite difference expression of the resulting equation is given by

$$\begin{aligned} \eta_{i,j}^{n+1} = & \left(\eta_{i,j}^n - \frac{\Delta t}{2\Delta x} \sum_1^N (q_{kx,i+1,j}^{n+2/3} - q_{kx,i-1,j}^{n+2/3}) - \frac{\Delta t}{2\Delta y} \sum_1^N (q_{ky,i,j+1}^{n+2/3} - q_{ky,i,j-1}^{n+2/3}) \right) \\ & + g\frac{\Delta t^2}{\Delta x^2} \left[\left(H + \frac{\eta_{i+1,j}^{n+1} + \eta_{i,j}^{n+1}}{2} \right) (\eta_{i+1,j}^{n+1} - \eta_{i,j}^{n+1}) - \left(H + \frac{\eta_{i,j}^{n+1} + \eta_{i-1,j}^{n+1}}{2} \right) (\eta_{i,j}^{n+1} - \eta_{i-1,j}^{n+1}) \right] \\ & + g\frac{\Delta t^2}{\Delta y^2} \left[\left(H + \frac{\eta_{i,j+1}^{n+1} + \eta_{i,j}^{n+1}}{2} \right) (\eta_{i,j+1}^{n+1} - \eta_{i,j}^{n+1}) - \left(H + \frac{\eta_{i,j}^{n+1} + \eta_{i,j-1}^{n+1}}{2} \right) (\eta_{i,j}^{n+1} - \eta_{i,j-1}^{n+1}) \right], \end{aligned} \tag{20}$$

where η_{ij} is the free surface elevation, i is the node number in the x-direction and j is the node number in the y-direction.

NON-LINEAR ADVECTION

The method used to solve the non-linear advection step is described in detail in this section.

For computational efficiency, equations (7)–(10) are further split into the one-dimensional system

$$\frac{\bar{q}_{kx}^{n+1/3} - q_{kx}^n}{\Delta t} + U_k \frac{\partial q_{kx}}{\partial x} = 0, \qquad \frac{q_{kx}^{n+1/3} - \bar{q}_{kx}^{n+1/3}}{\Delta t} + V_k \frac{\partial q_{kx}}{\partial y} = 0, \tag{21}$$

$$\frac{\bar{q}_{ky}^{n+1/3} - q_{ky}^n}{\Delta t} + U_k \frac{\partial q_{ky}}{\partial x} = 0, \qquad \frac{q_{ky}^{n+1/3} - \bar{q}_{ky}^{n+1/3}}{\Delta t} + V_k \frac{\partial q_{ky}}{\partial y} = 0, \tag{22}$$

$$\frac{\bar{k}_k^{n+1/3} - k_k^n}{\Delta t} + U_k \frac{\partial k_k}{\partial x} = 0, \qquad \frac{k_k^{n+1/3} - \bar{k}_k^{n+1/3}}{\Delta t} + V_k \frac{\partial k_k}{\partial y} = 0, \tag{23}$$

$$\frac{\bar{\epsilon}_k^{n+1/3} - \epsilon_k^n}{\Delta t} + U_k \frac{\partial \epsilon_k}{\partial x} = 0, \qquad \frac{\epsilon_k^{n+1/3} - \bar{\epsilon}_k^{n+1/3}}{\Delta t} + V_k \frac{\partial \epsilon_k}{\partial y} = 0. \tag{24}$$

From the Lagrangian point of view these equations describe the pure advection of velocities, k and ϵ. Hence these quantities should be invariant along the characteristic lines. Consequently, the location of the characteristic lines can be obtained from

$$dx/dt = U_\alpha^n, \qquad dy/dt = V_\alpha^n, \tag{25}$$

where

$$U_\alpha^n = U_i^n(1 - U_i^n \Delta t/\Delta x) + U_{i-1}^n U_i^n \Delta t/\Delta x, \qquad V_\alpha^n = V_j^n(1 - V_j^n \Delta t/\Delta y) + V_{j-1}^n V_j^n \Delta t/\Delta y$$

for U_i^n, $V_j^n > 0$ and a linear variation in velocity in space.

After the determination of the characteristic line the values of $q_{kx}^{n+1/3}$, $q_{ky}^{n+1/3}$, $k_k^{n+1/3}$ and $\epsilon_k^{n+1/3}$ at node (i, j, k) are obtained by interpolation of the nodal values at known time step n. However, the choice of interpolation function can have a significant effect on the accuracy of the solution. From the consideration of both accuracy and efficiency an efficient four-node minimax–characteristics scheme 4NMC for advection[7] was employed for the solution of the equations of pure advection. The 4NMC scheme uses a quadratic polynomial for interpolation over four nodes ($i-2$, $i-1$, i and $i+1$) subjected to a minimax criterion, which passes through ϕ_i^n, ϕ_{i-1}^n and with the algebraic difference (A_d) between the polynomial and ϕ_{i-2}^n equal and opposite in sign to that between the polynomial and ϕ_{i+1}^n (Figure 1).

For linear advection problems (equations (7)–(10)) in which the velocity is variable in time and space, the non-conservative form of 4NMC can be written as

$$\bar{\phi}_i^{n+1/3} = -0{\cdot}25v(1 - v)(\phi_{i-2}^n + \phi_{i+1}^n) + (1{\cdot}25v - 0{\cdot}25v^2)\phi_{i-1}^n + (1 - 0{\cdot}75v - 0{\cdot}25v^2)\phi_i^n, \tag{26}$$

where $v = U_\alpha^n \Delta t/\Delta x$ is assumed to be less than unity and $\phi = q_{kx}$, q_{ky}, k_k or ϵ_k; then

$$\phi_j^{n+1/3} = -0{\cdot}25v(1 - v)(\bar{\phi}_{j-2}^{n+1/3} + \bar{\phi}_{j+1}^{n+1/3}) + (1{\cdot}25v - 0{\cdot}25v^2)\bar{\phi}_{j-1}^{n+1/3} + (1 - 0{\cdot}75v - 0{\cdot}25v^2)\bar{\phi}_j^{n+1/3}, \tag{27}$$

where v changes to $v = V_\alpha^n \Delta t/\Delta y$, which is also assumed to be less than unity, and thus equations (7)–(10) are solved.

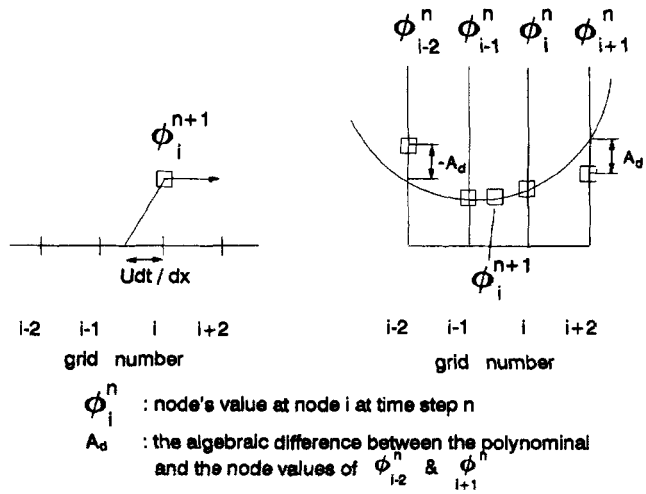

Figure 1. Illustration of 4NMC scheme

BOUNDARY CONDITIONS

The boundary conditions in the present model are specified as follows.

Upstream and downstream boundary conditions

In simulating the recirculating flow after a channel expansion, the location of the exit plane should be sufficiently far downstream of the section where the expansion exists so that the exit plane does not affect the separation and reattachment processes. If the computational domain is sufficiently long, the profiles of velocity and viscosity both upstream and downstream should become those of the fully developed channel flow. Thus we can apply zero-gradient conditions at both the inlet and outlet planes for all variables in simulating both the channel flow and the recirculating flow behind the expansion, except those variables which are assumed to be fixed.

In the upstream region the vertical variation in the longitudinal velocity U is specified as a logarithmic profile with Manning coefficient n, the transverse velocity V is assumed to be equal to zero and all other dependent variables, i.e. water depth, k and ϵ, are equal to the adjacent interior point values.

In the downstream region the water depth is specified and the velocities (U and V), k and ϵ are equal to the adjacent interior point values.

Wall boundary conditions

At solid wall boundaries a no-slip boundary condition is used and the wall function technique proposed by Launder and Spalding[11] is applied. According to this technique, the conditions are specified at a grid point which lies outside the laminar sublayer and the velocity at this grid point is given by the universal law of the wall,

$$\frac{U_w}{U_*} = \frac{1}{K_c}\ln(EY^+), \tag{28}$$

where $Y^+ = U_* y_n/\nu$ and

$$\tau_w/\rho = U_*^2. \tag{29}$$

Here τ_w is the wall friction stress, ρ is the ambient water density, U_w is the resultant velocity along the solid wall boundary, U_* is the resultant friction velocity, y_n is the normal distance between the first grid point and the wall, K_c is the Von Karman constant and E is a parameter representing the wall roughness which is assumed equal to unity.

In addition, assuming that the turbulence near the wall is in local equilibrium, the turbulent shear stress is approximately equal to the wall shear stress when the buoyancy effect is absent. Under this assumption, k and ϵ at the grid points next to the wall are given by[11]

$$k_w = \frac{U_*^2}{\sqrt{C_\mu}}, \qquad \epsilon_w = \frac{U_*^3}{K_c y_n} = \frac{U_*^4}{K_c \nu Y^+}. \tag{30}$$

Free surface boundary conditions

At the top layer the surface stresses τ_{sx} and τ_{sy} are assumed to be zero. The zero surface stresses imply that the surface tension and viscous effects are small and negligible,[13] which further implies that k and ϵ are zero.

Bottom boundary conditions

At the bottom layer the magnitudes of the bottom stresses τ_{bx} and τ_{by} are specified by the Manning equation and the values of k and ϵ at the grid points next to the bottom, k_b and ϵ_b, are defined by using the universal law of the wall:

$$\frac{\tau_{bx}}{\rho} = \frac{C_f}{2}\bar{U}(\bar{U}^2 + \bar{V}^2)^{1/2}, \qquad \frac{\tau_{by}}{\rho} = \frac{C_f}{2}\bar{V}(\bar{U}^2 + \bar{V}^2)^{1/2}, \tag{31}$$

where

$$\frac{C_f}{2} = \frac{gn^2}{H^{1/3}}, \tag{32}$$

$$U_{\tau x} = \sqrt{\left(\frac{\tau_{bx}}{\rho}\right)}, \qquad U_{\tau y} = \sqrt{\left(\frac{\tau_{by}}{\rho}\right)}, \tag{33}$$

$$k_b = \frac{U_\tau^2}{\sqrt{C_\mu}}, \qquad \epsilon_b = \frac{U_\tau^3}{K_c z_n} = \frac{U_\tau^4}{K_c \nu Z^+}. \tag{34}$$

Here n is Manning's coefficient, $Z^+ = U_\tau z_n/\nu$, which is similar to Y^+, $U_\tau^2 = U_{\tau x}^2 + U_{\tau y}^2$, $U_{\tau x}$ and $U_{\tau y}$ are the bottom friction velocities in the longitudinal and transverse directions respectively, U_τ is the resultant bottom friction velocity and z_n is the normal distance between the first grid point and the bottom.

SIMULATION RESULTS

Recirculating flows behind an obstruction are common occurrences in nature. Turbulence in the recirculating flows is generated by the transverse shear and the bed friction.[3] The large-scale turbulence generated by the transverse shear is characterized by the length scale of expansion width D. The small-scale turbulence generated by the bed friction is characterized by the length scale H/C_f. The bed friction stresses, besides generating turbulence, will exert a stabilizing influence on the transverse motion and hence reduce the turbulence generated. Therefore the effect of the bed friction is two-edged.

In this study, two dimensionless parameters C_f and D/H are chosen to investigate the effects of the turbulence generated by the bed friction and the transverse shear on the recirculating flows separately. The present model is employed to simulate the recirculating flows for a various values of C_f and D/H. The open channel to be simulated is 9·15–45·75 m wide, 0·1088–2·8080 m deep and 15·25–305 m long and the width of expansion is 2·2875–11·4375 m. The isometric view of the open channel with an expansion is shown in Figure 2. The inflow velocity at inlet is equal to 0·152 m s^{-1}. The time step is 0·02–0·1 s. The water body is cut into 10 layers of equal thickness and the computational region consists of a 9 × 30 mesh upstream of the abrupt expansion and a 31 × 40 mesh after the expansion. To generate a steady region of recirculation, about 30,000 iterations and approximately 460 min of CPU time on a Pentium 90PC are required.

The reattachment length of the recirculating flows, L, is selected for comparison since it is the most obvious measure of the recirculating flows. The computed reattachment lengths characterized by the expansion width are plotted against (i) $1/C_f$ for several values of D/H in Figure 3 and (ii) H/D for several values of C_f in Figure 4. It is observed that

(i) the reattachment length is proportional to $1/C_f$ for constant D/H
(ii) the reattachment length is proportional to H/D for constant C_f

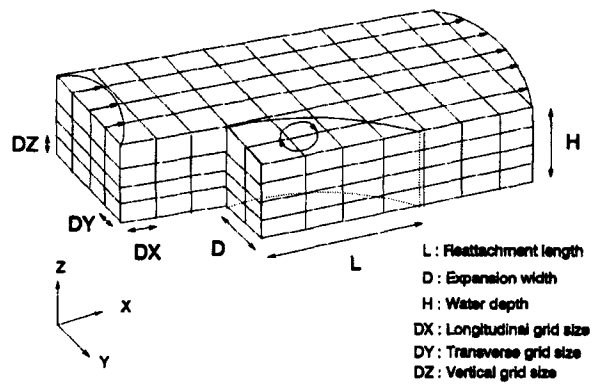

Figure 2. Isometric view of open channel with expansion

(iii) the reattachment length for any value of D/H will converge to a value equal to about eight times the expansion width if C_f is small enough
(iv) the reattachment length will converge to a smaller value as C_f becomes larger.

Besides the above two parameters C_f and D/H, Babarutsi *et al.*[9] also introduced the bed friction number $S = C_f D/2H$ to measure the influence of the turbulences generated by the transverse shear and bottom friction. In order to test the effect of the bed friction number S, the reattachment lengths computed by the present model, characterized by the expansion width, are plotted against D/H for various values of S in Figure 5. It is observed that for a constant S, (i) the reattachment length is approximately constant when D/H is larger than 10 and (ii) the reattachment length will start to decrease with D/H when D/H is about 10. This means that for a constant S the reattachment length will converge to a maximum value when D/H is large enough and the reattachment length will decrease with D/H when D/H is small. In addition, the maximum converged value for a constant S will decrease as S increases. Thus L/D may not be constant for a constant value of S. Hence S may not be a suitable dimensionless parameter to characterize the reattachment length of the recirculating

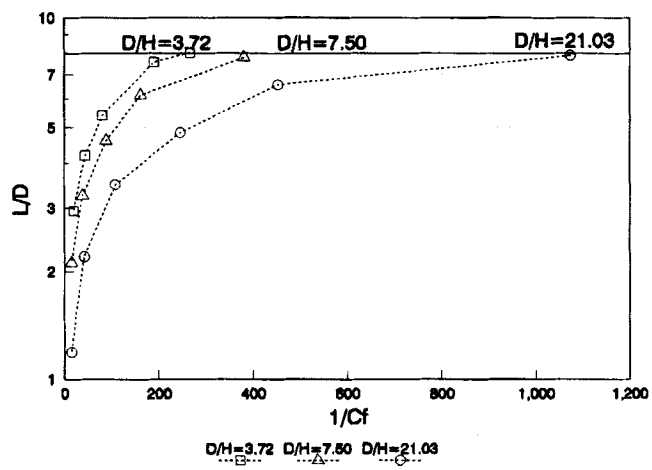

Figure 3. Computed L/D plotted against $1/C_f$ for various values of D/H

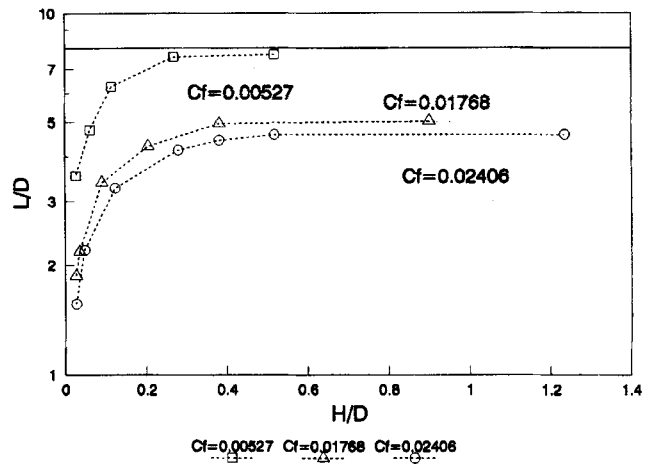

Figure 4. Computed L/D plotted against H/D for various values of C_f

flows. To compare the results computed by the present model and the data measured by Babarutsi *et al.*, the computed results and the measured data, which have the same values of C_f and D/H, are plotted against S in Figure 6. It is seen that the reattachment lengths predicted by the present model are in acceptable agreement with the measured data in the range of $S < 0{\cdot}02$ and $S > 0{\cdot}1$. Outside this range the reattachment length predicted by the present model is shorter than the measured one. This may be due to the inadequacy of the present model as well as the uncertainty of the experimental data.

For the purpose of comparison of the M$k\epsilon$ and D$k\epsilon$ models the relative recirculation lengths computed by them are plotted against $1/C_f$ at $D/H = 7{\cdot}50$ in Figure 7. It is observed that

(i) the results computed by the M$k\epsilon$ model are larger than those computed by the D$k\epsilon$ model when C_f is small

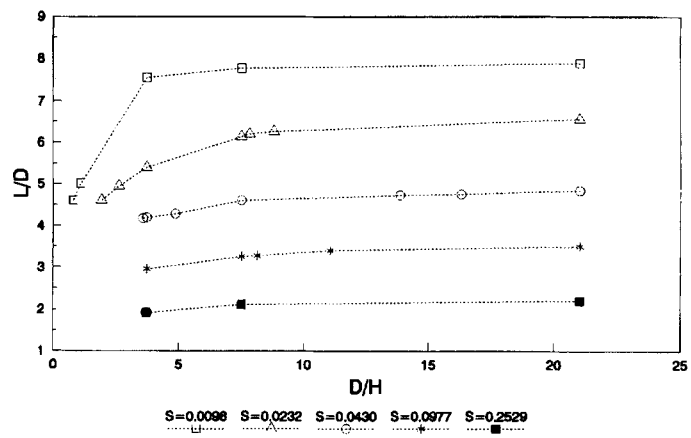

Figure 5. Computed L/D plotted against D/H for various values of S

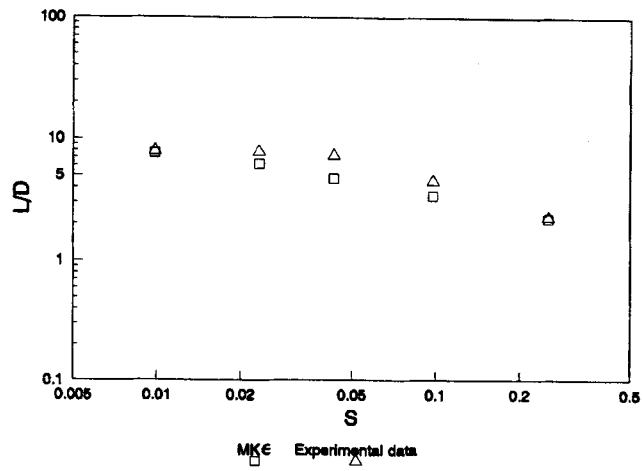

Figure 6. Comparison of L/D computed by M$k\epsilon$ model and measured data

(ii) L/D computed by the M$k\epsilon$ model tends to converge to 8·0 and L/D computed by the D$k\epsilon$ model tends to converge to a smaller value of about 6·0
(iii) the results computed by the M$k\epsilon$ model are approximately equal to those computed by the D$k\epsilon$ model when C_f is large.

To investigate the causes of the difference in the results computed by the two models, two cases, $C_f = 0{\cdot}00263$ (case 1) and $C_f = 0{\cdot}06744$ (case 2) at $D/H = 7{\cdot}50$, computed by M$k\epsilon$ are examined in detail, where case 1 represents a recirculating flow under a weak bottom friction and case 2 represents a recirculating flow under a strong bottom friction. To illustrate the typical flow field, the depth-averaged velocity distribution of the recirculating flows computed by M$k\epsilon$ for case 1 is shown in Figure 8. As marked in Figure 8, point 1 is located in the upstream region and point 2 is located in the

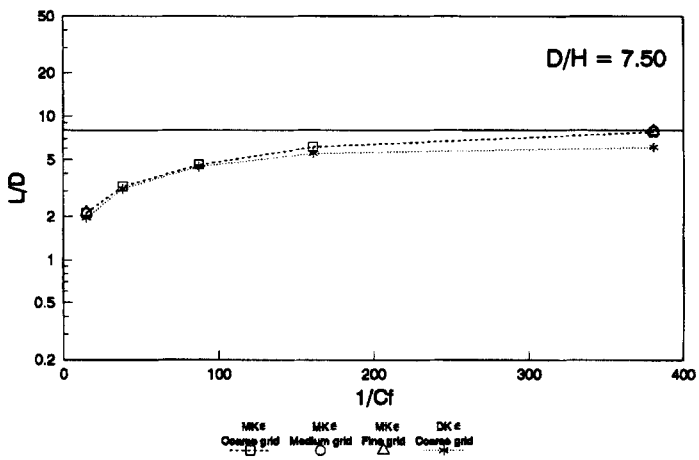

Figure 7. Comparison of L/D computed by M$k\epsilon$ and D$k\epsilon$ models

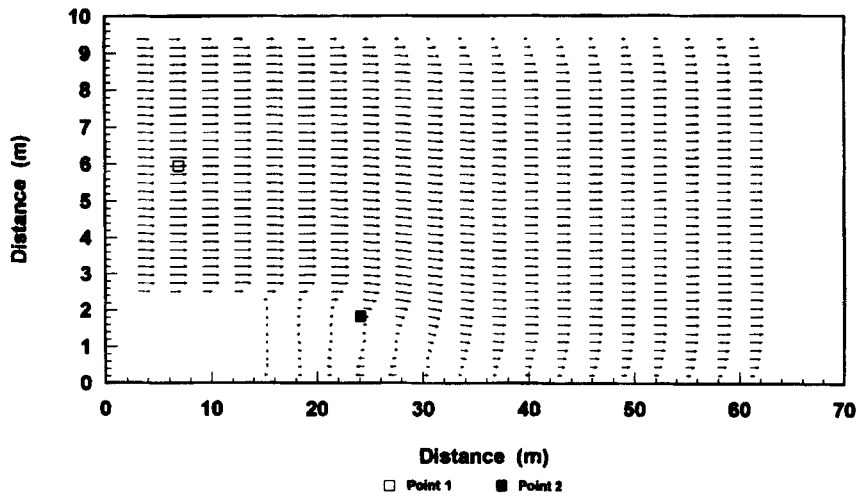

Figure 8. Depth-averaged flow field computed by M$k\epsilon$ model for case 1

recirculating zone. The vertical profiles of velocity and viscosity at points 1 and 2 of the two cases are illustrated in Figures 9 and 10 respectively.

For case 1 it is noted in Figure 9(b) that the vertical velocity profile at point 2 departs greatly from the typical logarithmic profile for open channel flow. In the D$k\epsilon$ model the values of k and ϵ in the water body are generated by two empirical terms P_{kv} and $P_{\epsilon v}$ (see Appendix 1) which are derived based on the logarithmic vertical velocity profile in uniform open channel flow. Thus, for flow with a vertical velocity profile which differs from the logarithmic profile, these empirical terms cannot give an accurate estimation of the bottom-generated turbulence there. Consequently, there is a large deviation between the results computed by the two models in case 1.

In case 2 the vertical velocity profiles both upstream and in the recirculation zone are relatively close to the logarithmic profile and thus the empirical terms in the D$k\epsilon$ model can give an accurate estimation of the bottom-generated turbulence there. Consequently, the results computed by the two models are close in case 2.

To demonstrate the convergence of the solutions in the horizontal directions, fine grid solutions are also computed for cases 1 and 2. The grid systems used in the channel expansion region for the simulation are 31 × 40 (the original coarse grid), 46 × 60 (medium grid) and 61 × 79 (fine grid). The computed recirculation lengths converge to within 1 per cent difference (Figure 7). In Figures 9 and 10 the computed vertical velocity and viscosity profiles also converge at point 1 which is in the main channel. At point 2 which is in the recirculation zone the convergence of the solution has not been achieved. A difference of over 10 per cent in the computed velocities (and about 5 per cent in the computed viscosities) is observed. This can be explained by the slight migration of the recirculation eddies in the simulations using different grid systems, which induces large inaccuracy for point-to-point comparison. As the computational time for the fine grid solution is excessive (about 61 h on the Pentium 90PC), carrying out the numerical simulation using an even finer grid has not been attempted.

Furthermore, to demonstrate the improvement in the solution with an increasing number of layers (N), the solutions of the two extreme cases 1 and 2 are further computed for $N=5$ and 20. The

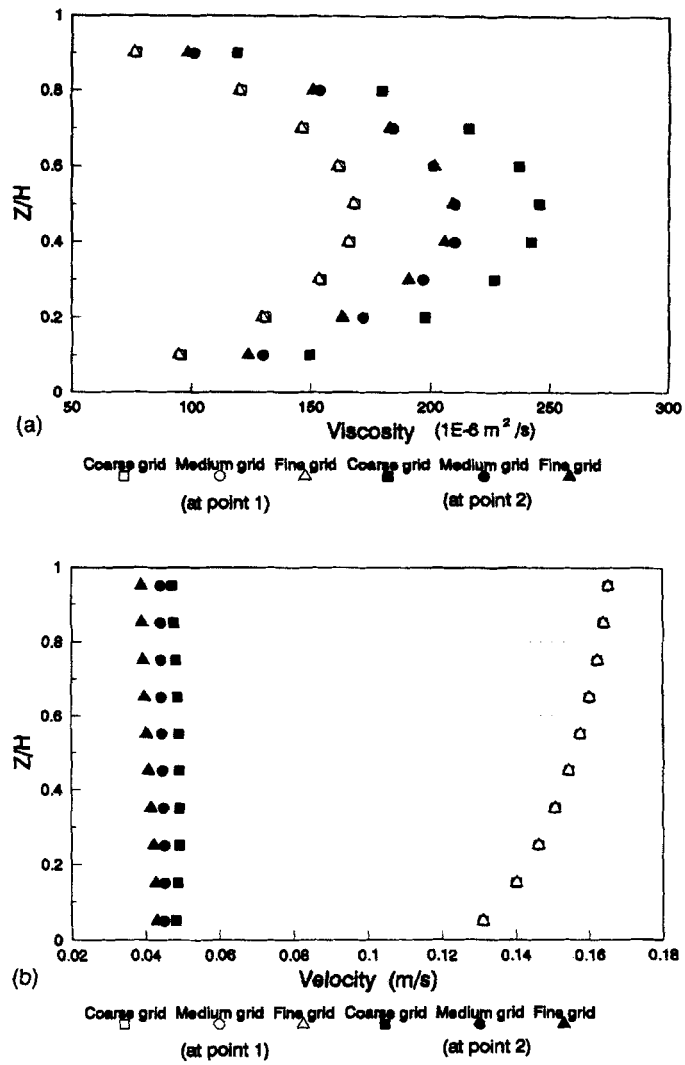

Figure 9. Vertical distributions of (a) viscosity and (b) longitudinal velocity U at points 1 and 2 for case 1

reattachment lengths and the vertical variations in viscosity and velocity computed for $N=1$ (depth-integrated model), 5, 10 and 20 for the two cases are presented in Table 1 and Figures 11 and 12. It is found that the reattachment lengths computed by the present model are converged for $N \approx 5$ (Table 1). The computed vertical profiles of longitudinal velocity converge to within 2 per cent difference (Figures 11(b) and 12(b)) and a difference of about 5 per cent in the computed viscosities for $N=10$ is observed (Figures 11(a) and 12(a)). Therefore it is sufficient to cut the water body into 10 layers in this study to obtain numerically accurate solutions.

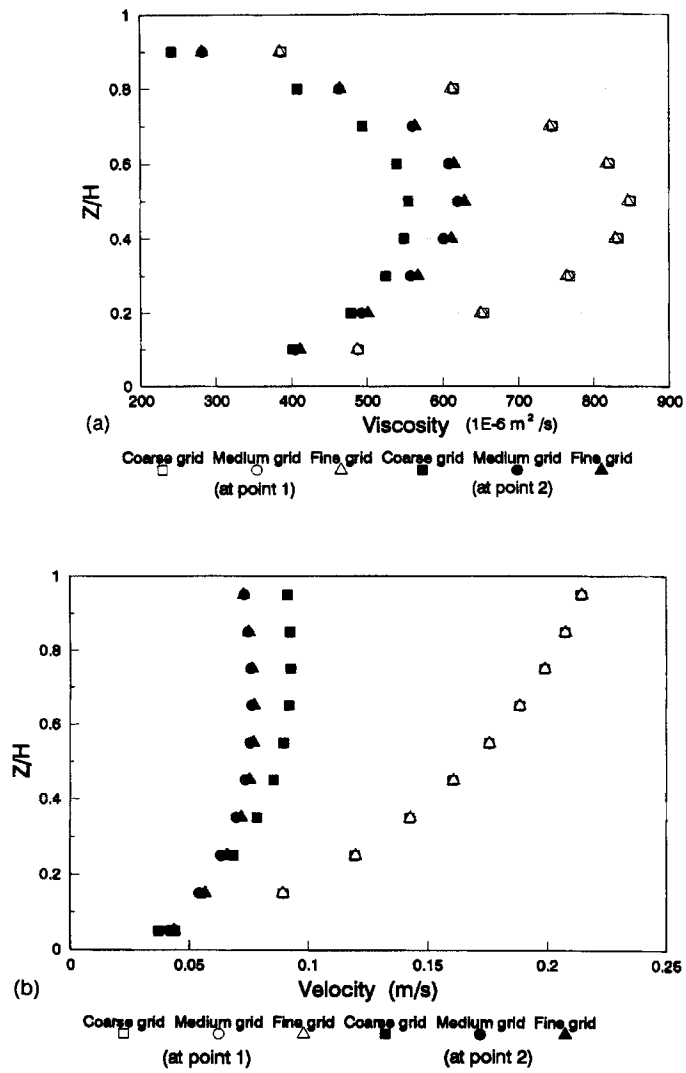

Figure 10. Vertical distributions of (a) viscosity and (b) longitudinal velocity U at points 1 and 2 for case 2

CONCLUSIONS

A quasi-three-dimensional multilayer $k-\epsilon$ model (M$k\epsilon$) which takes account of the vertical variation in velocities, k, ϵ and viscosity has been developed and applied to calculate the turbulent recirculation flows behind a sudden expansion in an open channel. The relative effect of bed-generated turbulence and transverse shear-generated turbulence on the recirculating flow has been studied. The results computed by the M$k\epsilon$ model are in closer agreement with the reported experimental data than are those computed by a depth-integrated $k-\epsilon$ model.

Table I. Effects of computed reattachment length on number of layers (N)

S	C_f	Number of layers (N)	L/D
0·0098	0·00263	1*	6·1
		5	7·8
		10	7·8
		20	7·8
0·2529	0·06744	1	2·0
		5	2·1
		10	2·1
		20	2·1

* When $N=1$, the $Dk\epsilon$ model is used.

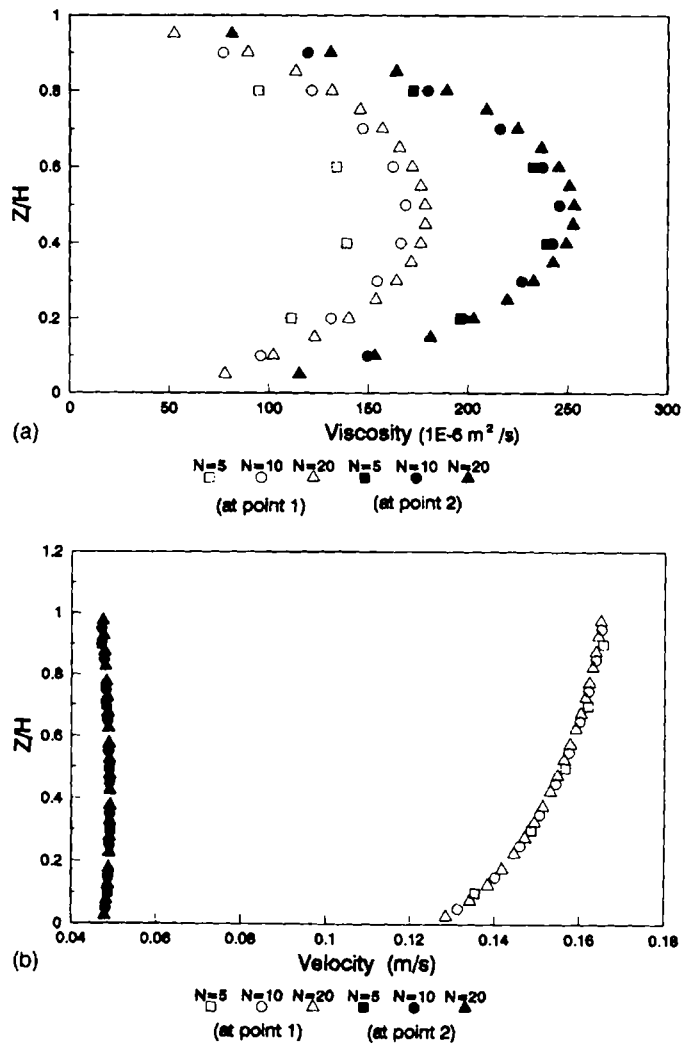

Figure 11. Illustration of convergence of computed solutions with number of layers (N) for case 1: vertical distributions of (a) viscosity and (b) longitudinal velocity U at points 1 and 2

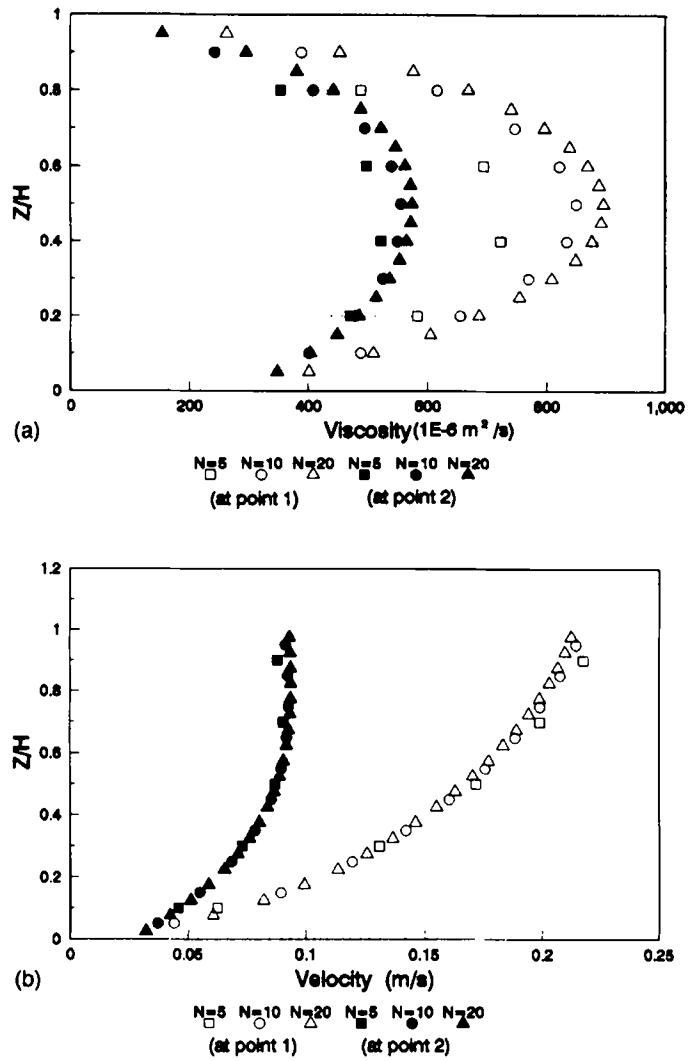

Figure 12. Illustration of convergence of computed solutions with number of layers (N) for case 2: vertical distributions of (a) viscosity and (b) longitudinal velocity U at points 1 and 2

APPENDIX

The $k-\epsilon$ equations of the depth-integrated $k-\epsilon$ (D$k\epsilon$) model[1] are

$$\frac{\partial \bar{k}}{\partial t}+\bar{U}\frac{\partial \bar{k}}{\partial x}+\bar{V}\frac{\partial \bar{k}}{\partial y}=\frac{\partial}{\partial x}\left(\frac{\bar{\nu}}{\sigma_k}\frac{\partial \bar{k}}{\partial x}\right)+\frac{\partial}{\partial y}\left(\frac{\bar{\nu}}{\sigma_k}\frac{\partial \bar{k}}{\partial y}\right)+P_h+P_{kv}-\bar{\epsilon},$$

$$\frac{\partial \bar{\epsilon}}{\partial t}+\bar{U}\frac{\partial \bar{\epsilon}}{\partial x}+\bar{V}\frac{\partial \bar{\epsilon}}{\partial y}=\frac{\partial}{\partial x}\left(\frac{\bar{\nu}}{\sigma_\epsilon}\frac{\partial \bar{\epsilon}}{\partial x}\right)+\frac{\partial}{\partial y}\left(\frac{\bar{\nu}}{\sigma_\epsilon}\frac{\partial \bar{\epsilon}}{\partial y}\right)+C_{1\epsilon}\frac{\bar{\epsilon}}{\bar{k}}P_h+P_{\epsilon v}-C_{2\epsilon}\frac{\bar{\epsilon}^2}{\bar{k}},$$

with

$$P_h = \bar{\nu}\left[2\left(\frac{\partial \bar{U}}{\partial x}\right)^2 + 2\left(\frac{\partial \bar{V}}{\partial y}\right)^2 + \left(\frac{\partial \bar{U}}{\partial y} + \frac{\partial \bar{V}}{\partial x}\right)^2\right],$$

$$P_{kv} = C_k \frac{U_\tau^3}{H}, \qquad P_{\epsilon v} = C_\epsilon \frac{U_\tau^4}{H^2}, \qquad U_\tau = \sqrt{[C_f'(\bar{U}^2 + \bar{V}^2)]},$$

where U_τ is the bottom friction velocity and C_f' is the friction coefficient. The empirical constants C_k and C_ϵ are determined from undisturbed normal channel flow as

$$C_k = \frac{1}{\sqrt{C_f'}}, \qquad C_\epsilon = 3{\cdot}6 \frac{C_{2\epsilon}}{(C_f')^{0{\cdot}75}} \sqrt{C_\mu}.$$

REFERENCES

1. W. Rodi, *Turbulence Models and Their Application in Hydraulics: A State-of-the-Art Review*. International Association for Hydraulics Research, Delft, 1980.
2. A. K. Rastogi and W. Rodi, 'Predictions of heat and mass transfer in open channels', *J. Hydraul. Div., ASCE*, **104**, 397–420 (1978).
3. R. Booij, 'Depth-averaged $k-\epsilon$ modelling', *Proc. 23rd IAHR Congr.*, Ottawa, 1989, pp. A199–A206.
4. L. R. Yu and S. N. Zhang, 'A new depth-averaged two-equation turbulent closure model', *Proc. 3rd Int. Symp. on Refined Flow Modelling and Turbulent Measurement*, Tokyo, 1988, pp. 549–555.
5. R. S. Chapman and C. Y. Kuo, 'Application of the two-equation $k-\epsilon$ turbulence model to a two-dimensional, steady, free surface flow problem with separation', *Int. j. numer. methods fluids*, **5**, 257–268 (1985).
6. N. N. Yanenko, *The Method of Fractional Steps*, Springer, New York, 1971.
7. C. W. Li, 'Advection simulation by minimax–characteristics method', *J. Hydraul. Eng., ASCE*, **9**, 1138–1144 (1990).
8. P. J. Roache, *Computational Fluid Dynamics*, Hermosa, Albuquerque, NM, 1976.
9. S. Babarutsi, J. Ganoulis and V. H. Chu, 'Experimental investigation of shallow recirculating flows', *J. Hydraul. Eng., ASCE*, **115**, 906–924 (1989).
10. J. O. Backhaus, 'A three-dimensional model for the simulation of shelf sea dynamics', *Dt. Hydrogr. Z.*, **38**, 165–186 (1985).
11. B. E. Launder and D. B. Spaulding, 'The numerical computation of turbulent flows', *Comput. Methods Appl. Mech. Eng.*, **3**, 269– 289 (1974).
12. J. P. Benqué, J. A. Cunge, J. Feuillet, A. Hauguel and F. M. Holly. 'A new method for tidal current computation', *J. Waterways Harbours Div., ASCE*, **108**, 396–417 (1981).
13. H. B. Fischer, E. J. List, R. C. Y. Koh, J. Imberger and N. H. Brooks, *Mixing in Inland and Coastal Waters*, Academic, New York, 1979.